ACS OMEGA

http://pubs.acs.org/journal/acsodf

Article

Long-Term and Stable Dental Therapies *via* an In Situ Spontaneous Medicine Delivery System

Xuan Heng, Yuhao Pan, Xinghui Chen, Liuyi Pu, Jiaping Lu,* Ka Li,* and Kangjian Tang*

Cite This: *ACS Omega* 2023, 8, 23936−23944

Read Online

ACCESS | Metrics & More | Article Recommendations | Supporting Information

ABSTRACT: Chronic oral diseases are boring, long-term, and discomfort intense diseases, which endanger the physical and mental health of patients constantly. Traditional therapeutic methods based on medicines (including swallowing drugs, applying ointment, or injection in situ) bring much inconvenience and discomfort. A new method possessing accurate, long-term, stable, convenient, and comfortable features is in great need. In this study, we demonstrated a development of one spontaneous administration for the prevention and therapy on a series of oral diseases. By uniting dental resin and medicine-loaded mesoporous molecular sieve, nanoporous medical composite resin (NMCR) was synthesized by a simple physical mixing and light curing method. Physicochemical investigations of XRD, SEM, TEM, UV−vis, N_2 adsorption, and biochemical experiments of antibacterial and pharmacodynamic evaluation on periodontitis treatment of SD rats were carried on to characterize an NMCR spontaneous medicine delivery system. Compared to existing pharmacotherapy and in situ treatments, NMCR can keep a quite long time of stable in situ medicine release during the whole therapeutic period. Taking the periodontitis treatment as an instance, the probing pocket depth value in a half-treatment time of 0.69 from NMCR@MINO was much lower than that of 1.34 from the present commercial Periocline ointment, showing an over two times effect.

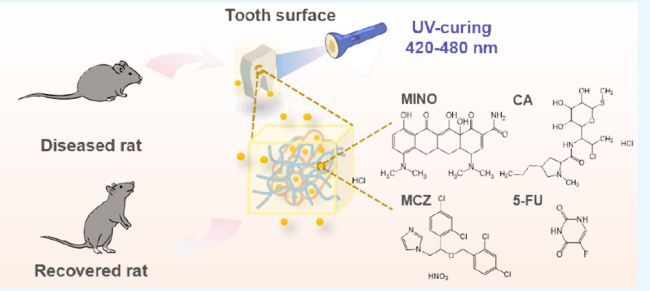

1. INTRODUCTION

Periodontal diseases, dental caries (cavities), oral mucosal diseases, and lip and oral cancers are among the most prevalent and chronic oral diseases (COD) worldwide.[1,2] A survey reported that the number of people suffering from these oral diseases directly reached from 2.5 billion to as high as 3.5 billion from the year of 1990 to 2019. More than 44.5% of the global population suffered their indirect influences as well. The unwilling economic expenditure, up to tens of billions of U.S. dollars, had to be paid for onerous COD therapies every year.[3,4] It is predicted that the prevalence of oral diseases will increase with global population growth in the coming decades.[5,6] Aiming on traditional COD therapies, there are three main methods of administration.[7] First is systemic administration, such as swallowing drugs (and then getting an effect through systemic circulation).[8] Second is applying ointment, and the third is injection on the affected part. Unfortunately, to reach and maintain effective medicine concentrations at the lesion site, high doses are often used by systemic delivery of medicines, which may lead to toxic gastrointestinal intolerance and resistance.[9,10] Applying ointments is not readily to make its residual at the target site, which would restrict the normal dietetic behaviors and lead to a strong foreign body sensation.[11,12] Injections have to be increased for open wounds and the presence of foreign bodies in the subgingival pocket. Constant severe pain is accompanied by local swelling. Worse, the injections cannot stay in the therapy area for a long time, which need to be reinjected every week.[13] All the mentioned facts bring quite inconvenience and discomfort, even more hurt, to patients during the treatment stage, which disturb seriously patients' normal social activities and reduce greatly the quality of life.[14] Therefore, aiming the specificity of the oral environment, the dietary needs of patients, and the comfort level of treatment, a promising strategy with accurate, long-term, stable, convenient, and even in situ spontaneous medicine delivery merits is in great need.

Precise medicine delivery systems had the advantages of high therapeutic efficiency, uninterrupted action, and low organ toxicity, which have been attracting widespread attention from the medical and chemical communities. Many successful delivery systems have been developed, such as chitosan in cancer, hydrogels in diabetic diseases, liposomes in Alzheimer's disease, and iron oxide nanoparticles in neoplastic diseases.[15−23] Mesoporous molecular sieve (MMS) is designed as one of the most ideal medicine delivery materials due to its adjustable pore size, large surface area, easily modified surface,

Received: April 10, 2023
Accepted: June 2, 2023
Published: June 17, 2023

Scheme 1. Schematic of Effective Release of Four Oral Disease Therapeutic Drug Molecules in the Oral Environment

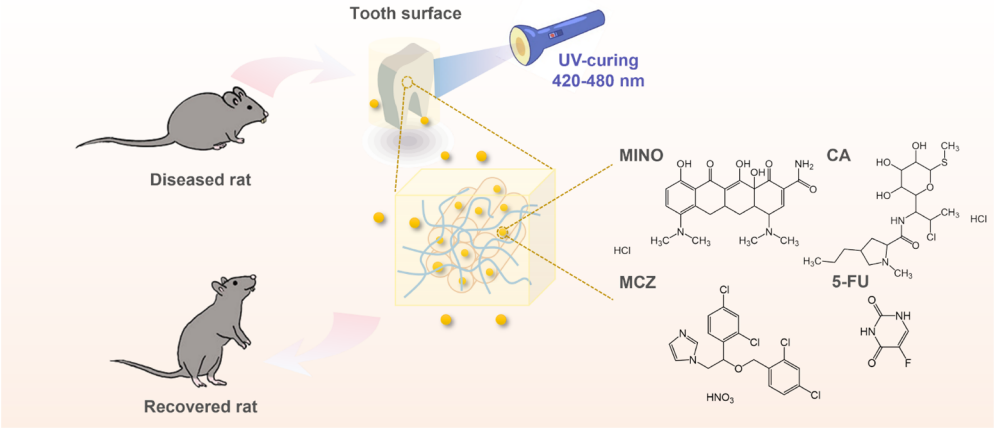

and excellent biocompatibility. Examples include the combination with hydrogels for myocardial infarction, with liposomes for cancer chemotherapy, with gold nanorods for tumor therapy, and with chitosan for gene therapy.[24−30] Methyl methacrylate resin (MMR) has a similar color and texture as a natural tooth, which is often used in dental restoration as a denture base material.[31−34] The motivation is to, through combining MMS and MMR, form effective medicine carriers and set up some vectors to achieve local, precise, and durable medicine release in the oral environment, hoping to achieve effective treatment on COD.

In this study, we demonstrate a development of one spontaneous administration for the prevention and therapy on a series of oral diseases. By uniting MMR and medicine-loaded SBA-15, one of the famous MMSs, nanoporous medical composite resin (NMCR), was synthesized by a simple physical mixing and light curing method. Compared to existing pharmacotherapy and in situ treatments, NMCR can keep a very long time of stable in situ medicine release during the therapeutic period (Scheme 1). Here, aiming the treatment of periodontitis, dental caries, oral ulcer, and mucosal carcinoma, we prepared four types of NMCR as a spontaneous delivery platform. The administration loading minocycline hydrochloride (MINO), clindamycin hydrochloride (CA), miconazole nitrate (MCZ), and 5-fluorouracil (5-FU) was expressed as NMCR@MINO, NMCR@CA, NMCR@MCZ, and NMCR@5-FU, respectively. The structures, morphologies, BET surface, and medicine release behaviors were investigated. The antimicrobial properties and in vivo pharmacodynamic evaluation on periodontitis treatment were evaluated. Compared to existing pharmacotherapy and in situ treatments, NMCR can keep a very long time of stable in situ medicine release during the therapeutic period.

2. MATERIALS AND METHODS

2.1. Materials. Medium and Australian premium fetal bovine serum (iCell-0500) were purchased from Cybikang. The MTT cell proliferation detection kit was purchased from Beijing Solaibao Technology. KB cells, *Streptococcus mutans*, *Actinomyces viscosus*, and *Candida albicans* were purchased from Cybikang (Shanghai, China). SD rats were purchased from Spife Biotechnology (Suzhou, China). EO_{20}-PO_{70}-EO_{20} (Pluronic P123, Ma = 5800) was purchased from Sigma-Aldrich. The 3M resin of Filtek-Z250 was purchased from 3M. The MINO, CA, MCZ, 5-FU, and other chemical compounds were purchased from Macklin. The multifunction microplate reader (TECAN SPARK 10M) was purchased from Ruishang. The clean bench (SW-CJ-2FD) was purchased from Sujing Antai.

2.2. Characterization. Transmission electron microscopy (TEM) analysis was performed on an American FEI Tecnai G20. X-ray diffraction (XRD) analysis was carried out on a German Brook D8 Advance. Scanning electron microscopy (SEM) analysis was carried out on a Czech TESCAN VEGA 3 SBH. The UV−vis spectrum was measured on a Shimadzu UV3600. The Fourier transform infrared (FT-IR) spectrum was measured on a Nicolet 6700 from Thermo Fisher Technology. The high-temperature and high-pressure steam sterilization pot (HVE-50) was purchased from Hirayama. The constant-temperature oscillator (crystal IS-RDV1) was purchased from American Jing-qi.

2.3. Methods. *2.3.1. Synthesis of SBA-15.* The synthesis of SBA-15 with different pore sizes was referred to some previous studies.[35−37] Pluronic P123 (2.0 g) was dissolved in 57.0 g of water and 10 mL of 12 M HCl solution with stirring at 35 °C until completely dissolved. Then, stirring was continued with or without 0.4 g of 1,3,5-trimethylbenzene (TMB) as an expanding agent for 2 h. Tetraethyl orthosilicate (4.3 g) was added dropwise into the mixed solution and stirred at 38 °C for 24 h. Then, the precursor was transferred into a Teflon-lined stainless-steel autoclave and crystallized at 100 °C for 48 h. The sample was filtered, washed with deionized water, and dried at 60 °C overnight. To remove the surfactant template, the dried product was heated from room temperature (RT) to 550 °C at a heating rate of 2 °C/min, followed by calcination in air for 6 h. Finally, SBA-15 white powders with different pore sizes were obtained and named SBA-15-1 (0.4 g of TMB) and SBA-15-2 (no TMB).

2.3.2. Preparation of Medicine Stock Solution. MINO or CA (0.2 g) was dissolved in 10 mL of water to obtain MINO or CA solution with a concentration of 20 mg/mL at RT. The max wavelength (λ_{max}) of UV absorption was 222 nm by MINO solution and 202 nm by CA solution; 0.10 g of MCZ or 5-FU was dissolved in 10 mL of ethanol to obtain MCZ or 5-FU ethanol solution with a concentration of 10 mg/mL. The λ_{max} was 205 nm for MCZ and 265 nm for 5-FU.

2.3.3. Medicine Loading. SBA-15 loaded with medicines was obtained by a solvent impregnation method.[38] Taking the load of MINO as an example, 0.5 g of SBA-15-1 was added to

https://doi.org/10.1021/acsomega.3c02428
ACS Omega 2023, 8, 23936−23944

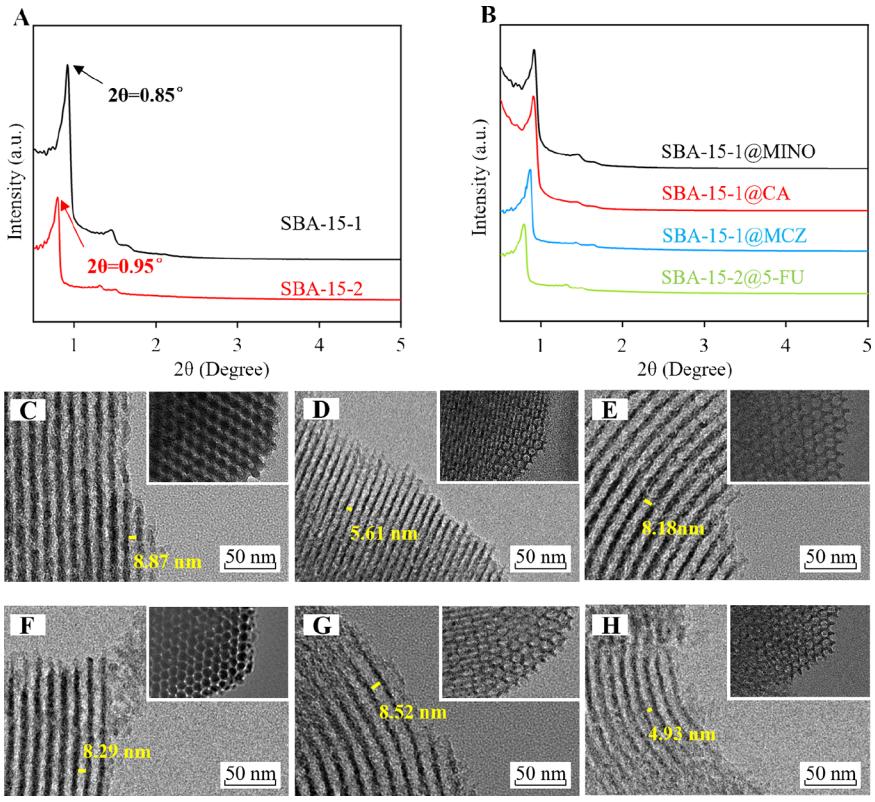

Figure 1. XRD patterns of (A) SBA-15-1 and SBA-15-2 and (B) SBA-15 after loading different medicines; TEM images of (C) SBA-15-1, (D) SBA-15-2, (E) SBA-15-1@MINO, (F) SBA-15-1@CA, (G) SBA-15-1@MCZ, and (H) SBA-15-2@5-FU. The inset is the top view with the same scale bar.

10 mL of MINO aqueous solution and the suspension was stirred vigorously at RT for 24 h to achieve an equilibrium steady state. Then, the suspension was centrifuged at 6000 rpm for 20 min. The supernatants were collected and extracted into a quartz colorimetric ware with a 0.22 μ filter syringe. The solid powders were kept at 60 °C for 24 h for solvent evaporation. The sample was named SBA-15-1@MINO. The same methods were used to load CA and MCZ, named as SBA-15-1@CA and SBA-15-1@MCZ. Because the 5-FU molecule is much smaller than previous three molecules, SBA-15-2 without an expanding agent was selected as a 5-FU carrier, named as SBA-15-2@5-FU.

2.3.4. Preparation of Medicine-Loaded NMCR. Four groups of NMCRs loading MINO, CA, MCZ, and 5-FU individually were prepared, expressed as NMCR@MINO, NMCR@CA, NMCR@MCZ, and NMCR@5-FU, respectively. The preparation of NMCR@MINO was taken as an example. SBA-15-1@MINO (0.01 g) was mixed with resin (0.1 g) by physical stirring for 20 min. The sample was placed in the steel mold, and the sheet was pressed for 30 s at a pressure of 60 kg/cm^2. A hole punch was used on the sample sheet to the wafer sample (6 ± 1 mm in diameter), and the wafer sample was irradiated under UV light (420−480 nm) for curing in 60 s. The same method was used to prepare NMCR@CA, NMCR@MCZ, and NMCR@5-FU, respectively.

2.3.5. In Vitro Medicine Release Study. The wafer of medicine-loaded NMCR was accurately weighed and soaked in a sealed colorimetric ware containing 3 mL of PBS (pH = 7.2). The released medicine was recorded by a UV−vis spectrophotometer every 30 min at λ_{max}. All the experiments were performed in triplicate, and the results were reported as average. The percentage of medicine released was calculated by eq 1 below:

$$\text{Percentage of medicine release}(\%) = \frac{Q_t}{Q_0} \times 100\% \quad (1)$$

where Q_t is the cumulative amount of medicine released at time and Q_0 is the initial amount of medicine loaded. Measurements are made at RT under static conditions.

2.3.6. Antibacterial Activity. Some Luria-Bertani medium was imprinted in a Petri dish, on which 100 μL of fluid of *Viscous actinomycetes* was spread. A round disk made of 30 mg of NMCR@MINO was sterilized at high temperatures for 20 min and placed in the center of this Petri dish after cooling down the disk to RT. The Petri dish was incubated at 37 °C. At certain intervals, the growth of bacteria and the diameter of the inhibition zone were recorded to determine the antibacterial activity of NMCR@MINO. By using the same method, the determination of antibacterial activity on NMCR@CA and NMCR@MCZ was carried out on *S. mutans* in brain-heart infusion medium and *C. albicans* in yeast peptone dextrose medium.

2.3.7. In Vitro Cell Propagation Experiment. KB cells were seeded in a 96-well plate and incubated with 100 μL of medium at RT for 24 h. Then, the original medium was replaced by that with 5-FU and NMCR@5-FU, respectively. KB cells were incubated sequentially in these fresh mediums for 6, 12, 24, and 48 h. One hundred microliters of 5 mg/mL MTT reagent was added in, continuing incubation at CO_2 to 5%, 37 °C for 4 h. After removing the medium, 20 μL of DMSO was added into wells, shaking and incubating at RT for

https://doi.org/10.1021/acsomega.3c02428
ACS Omega 2023, 8, 23936−23944

Table 1. Physicochemical Properties of SBA-15 with and without Medicine Loading

samples	SBA-15-1	SBA-15-2	SBA-15-1@MINO	SBA-15-1@CA	SBA-15-1@MCZ	SBA-15-2@5-FU
surface area (m^2/g)	564.71	702.18	432.74	424.93	441.56	511.39
pore size (nm)	8.9	5.6	8.3	8.2	8.5	4.9

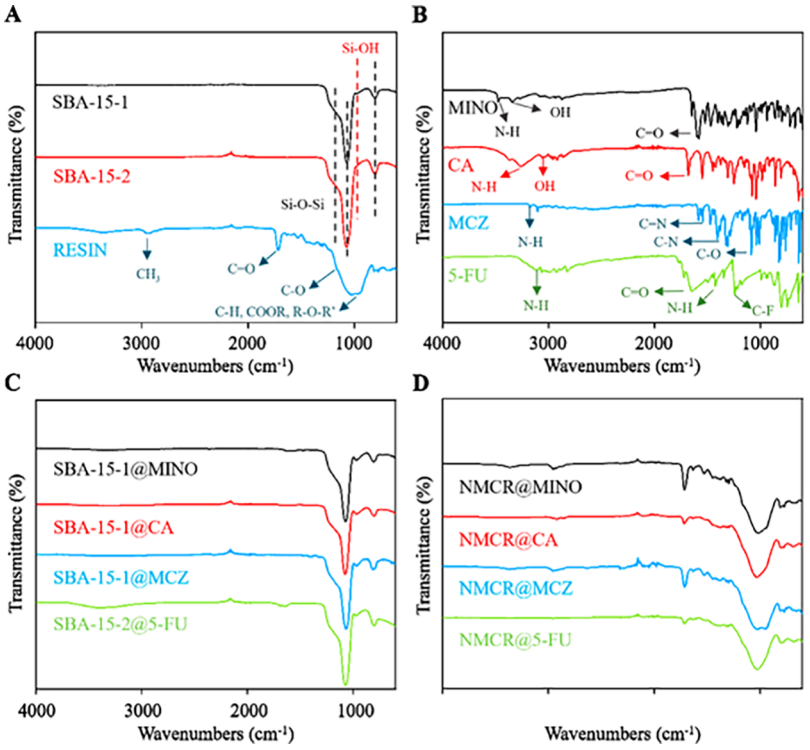

Figure 2. FT-IR spectra of (A) SBA-15-1, SBA-15-2, and resin, (B) four kinds of medicines with featured absorptions, (C) SBA-15-1 loading MINO, CA, and MCZ and SBA-15-2 loading 5-FU and (D) NMCR containing different medicines.

15 min away from light. The optical density (OD) of KB cells was measured with the enzyme-labeling method at an excitation wavelength of 570 nm. The cell activity was calculated by eq 2 below:

$$\text{Cell activity}(\%) = \frac{OD_t - OD'}{OD_0 - OD'} \times 100\% \quad (2)$$

where OD_t is the OD value of the experiment group, OD_0 is the OD value of the untreated control group, and OD′ is the OD value of the blank background plate.

2.3.8. Animal Experiment on the Establishment of the Periodontitis Model. The 7-week-old male Sprague−Dawley (SD) rats were randomly assigned into three groups: (1) control (normal) group, (2) model (ligation) group, and (3) sample (ligation + NMCR@MINO) group. Three percent sodium pentobarbitone (35 mg/kg) was used to anesthetize rats, and the first molar of the maxilla of the rats was ligated with a fine stainless-steel wire for 4 weeks. If the ligation became loose or fair, it was replaced immediately. One week later, *Viscous actinomycetes* and *S. mutans* were applied to the mouth of the ligation sites five times every other day. During this period, rats were fed a high-sugar viscous soft diet and 10% sucrose water. The control group did not experience this procedure. Then, the stainless-steel wires were removed and left untreated in the periodontitis rats (model group), whereas NMCR@MINO (approximately containing 0.36 mg of MINO) was applied to the tooth surface and cured under UV light immediately after removing ligation. The infiltration status of inflammatory cells and cementum integrity were further analyzed by a light microscope.

2.3.9. Statistical Analysis. The data was expressed as mean ± standard deviation (SD). Statistical analysis was performed with SPSS 22.0 (SPSS, Inc., Chicago, IL, USA). The two-group and multiple-group statistical analysis was compared by single-factor analysis of variance and *t*-test. $P < 0.05$ was considered to be statistically significant.

3. RESULTS AND DISCUSSION

3.1. Synthesis and Characterization. The structures of samples were recorded by the characterization methods of powder X-ray diffraction (pXRD) and TEM. The pXRD patterns of the synthesized materials are shown in Figure 1A,B. Figure 1A displays two curves with a strong peak at 2θ around 0.8 and 0.95° and two weak peaks in the range of 1.2 to 1.8°; these peaks can be indexed to the (100), (110), and (200) surfaces of the well-ordered hexagonal SBA-15 structure. SBA-15-1 has a smaller pore size of 5.6 nm, and SBA-15-2 has a larger pore size of 8.9 nm. Figure 1B displays four curves that correspond to MINO, CA, MCZ infusing in SBA-15-1, and 5-FU in SBA-15-2, respectively. Every curve has the feature peaks of SBA-15. Lower intensity than original samples reflect the effect of medicine infusion, illustrating that the medicine entered the pores but did not damage the porous structures. An obvious TEM observation of pore structures from Figure 1C−H verified the pXRD results. Figure 1C,D reveals the structures of two pure SBA-15 samples with different pore

https://doi.org/10.1021/acsomega.3c02428
ACS Omega 2023, 8, 23936−23944

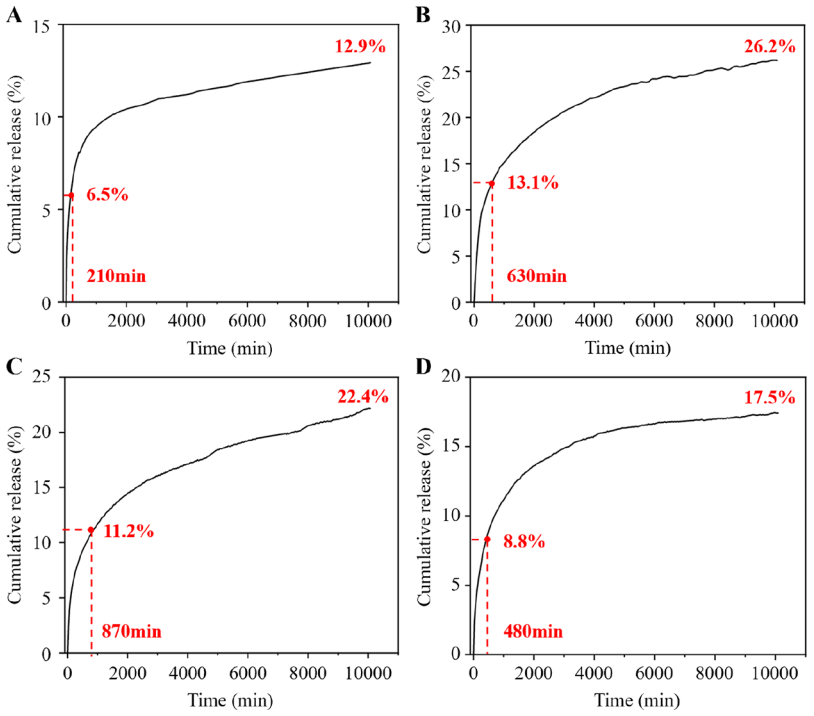

Figure 3. Time-dependent UV adsorption curves of (A) NMCR@MINO, (B) NMCR@CA, (C) NMCR@MCZ, and (D) NMCR@5-FU in PBS solution.

sizes. The diameter of SBA-15-1 and SBA-15-2 was measured at 8.87 and 5.61 nm, respectively. Figure 1E−H shows the records after infusing medicine. The length between two walls in four samples was measured at 8.18, 8.29, 8.52, and 4.93 nm, which means that there was a little pore contraction after infusion. It could be assumed that the medicine entered the pores effectively. All the observations of cross section were placed in insets. The overall morphology of these six samples was also recorded by SEM (Figure S1). The original SBA-15 samples had a rod-like shape and no obvious changes on the morphology after infusion of medicines.

N_2 adsorption−desorption isotherms were measured at 77 K to evaluate the infusing degree of medicines. Table 1 lists the surface areas and pore sizes of two SBA-15 and four medicine-loaded SBA-15 samples. With medicine loading, the surface area of SBA-15-1 decreased by 23.37, 24.75, and 21.81% and the pore size contracted by 6.7, 7.8, and 4.5% corresponding to @MINO, @CA, and @MCZ, respectively. The surface area and pore size of SBA-15-2 decreased by 27.17 and 12.5% after 5-FU infusion. Combined with TEM observation and BET results, it can be speculated that the existence of these four types of medicine molecules in SBA-15 was adsorbing to the inner and outer surfaces.

The states of surface groups on all involved compounds and materials were recorded by an FT-IR spectrometer. Figure 2A shows the characteristic IR spectra of base materials, SBA-15-1, SBA-15-2, and self-curing resin. Both the two SBA-15 samples have the same IR signature; the peaks located around 1220, 1074, and 804 cm^{-1} could be attributed to the vibration stretching and bending modes of Si−O−Si bonds. The peak at 972 cm^{-1} could be attributed to the vibration bending modes of the Si−OH groups. The main components of self-curving resin include bisphenol A-glycidyl methacrylate and triethylene glycol dimethacrylate. The vibration peaks at 2930, 1718, and 1168 cm^{-1} correspond to CH_3, C=O, and C−O groups. The broad peaks at 950−1150 cm^{-1} correspond mainly to C−H, COOR, and R−O−R′ groups. Figure 2B shows the infrared spectra of the four medicine molecules used in the delivery system. The labeled peaks show the functional groups of the corresponding medicines to study the interaction between mesoporous SBA-15 and medicines. As seen, MINO has N−H, OH, and C=O featured peaks at 3473, 3350, and 1581 cm^{-1}; CA has N−H, OH, and C=O featured peaks at 3264, 3064, and 1681 cm^{-1}; MCZ has N−H, C=N, C−N, and C−O featured peaks at 3182, 1477, 1332, and 1085 cm^{-1}; and 5-FU has N−H, C=O, and C−F featured peaks at 3134, 1664, and 1248 cm^{-1}, respectively.[39−42] Usually, the group of OH and N−H shows wavenumbers around 2500−3400 and 3100−3500 cm^{-1}, respectively. In this figure, some functional groups show a slight shift because these groups were affected by nearby groups such as benzene groups' vibration or the influence of hydrogen bonds.

Figure 2C reveals the graft state when the medicine was infused into SBA-15 pores. The featured absorption peaks of SBA-15 perfectly matched that shown in Figure 2A, but all the peaks from medicines vanished nearly. It implies that the adsorption of medicine in SBA-15 resulted in almost all the groups of N−H and O−H of medicine molecules connecting to part Si−OH groups of SBA-15. Figure 2D shows the IR spectra of these four medicine delivery systems by combining resin and medicine-loaded SBA-15. Only resin features could be indexed. Combined with these IR spectra and SEM observations (see Figure S2), the SBA-15@medicines should be fully encased by resin. Furthermore, the dispersion of N and F elements not contained in the resin was used to verify the overall dispersion of medicine-loaded SBA-15 by EDS characterization. As shown in Figure S3, the dispersion of SBA-15 in the resin is excellent, and no agglomeration is found.

3.2. In Vitro Studies on Sustained Medicine Release.

The releasing behaviors of MINO, CA, and MCZ molecules

https://doi.org/10.1021/acsomega.3c02428
ACS Omega 2023, 8, 23936−23944

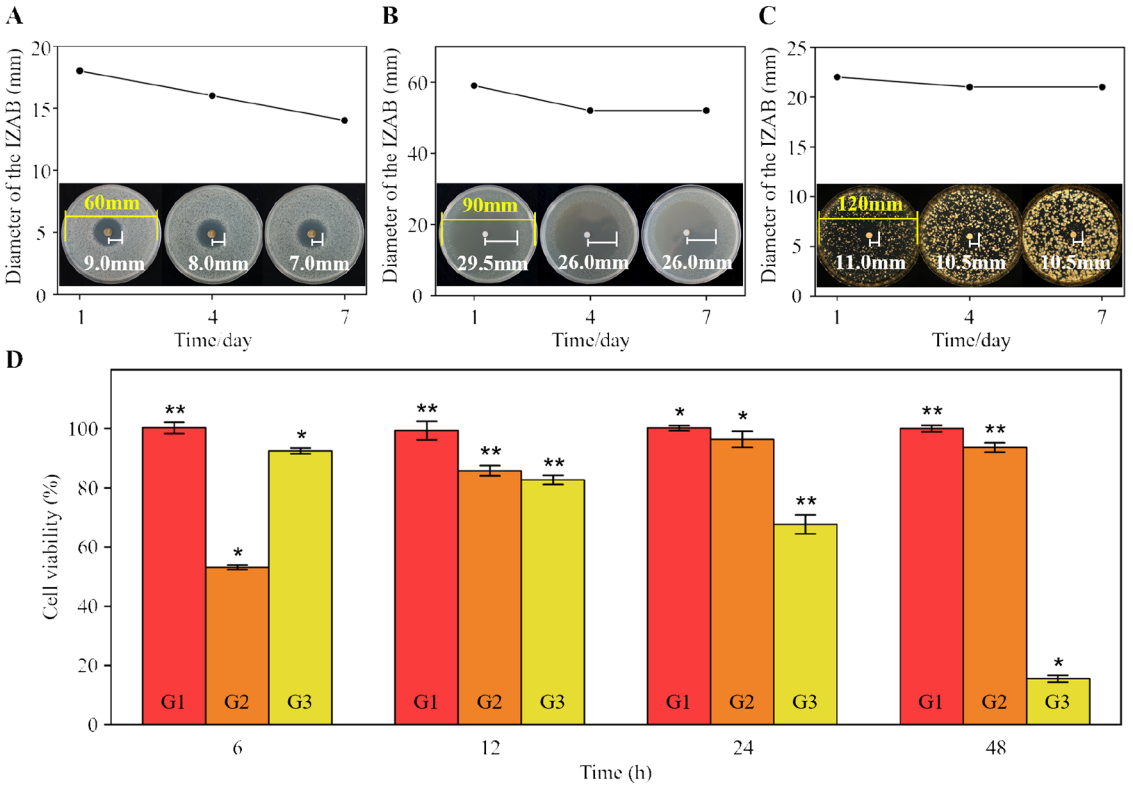

Figure 4. Photograph of the inhibition zone of (A) NMCR@MINO, (B) NMCR@CA, and (C) NMCR@MCZ (three kinds of Petri dishes with diameters of 60, 90, and 120 mm were used to culture different species of bacteria). (D) Percentage plot of cell growth.

from NMCRs were investigated in phosphate buffer (PBS) at pH 7.2, respectively. Figure 3 shows the medicine release curves to time, where the four curves have similar two-staged releasing profiles within 10,000 min. In the beginning, half amounts of medicines about 6.5% MINO, 13.1% CA, 11.2% MCZ, and 8.8% 5-FU were dissolved quickly from SBA-15 at the times of 210, 630, 870, and 480 min, respectively. The concentration of medicine in solution increased quickly, and the results corresponded to the very sharp upward curves in figures. Then, they were involved into long sustained release processes. The concentration of medicine in solution increased steadily, corresponding to gently rising curves. As seen, even testing at the 7th day (10,080 min), only 12.9% MINO, 26.2% CA, 22.4% MCZ, and 17.5% 5-FU were released. By using MINO as comparison, the releasing behaviors of SBA-15-1@MINO and RESIN@MINO were tested (see Figure S4) under the same releasing conditions. On SBA-15-1@MINO, the concentration of MINO in solution stopped increasing after a quick dissolution in 80 min, 45.2%.

MINO was released by calculation. That is to say, the MINO molecule can be free in and out of SBA-15 pores. Based on the 100% amount adsorbed into pores, about 45% could be released indeed but hard for the rest 55% to be released under RT conditions. On the contrary, only 12.8% MINO could be released from the RESIN@MINO system in a shorter time of 60 min, then stopping the release. That means that most of the MINO molecules were trapped in resin with some strong interactions between active chemical groups. Fortunately, while curving resin wrapped SBA-15 as a porous coat, the releasing behavior could be effectively controlled. It would be expected that the therapy can cover 3.5 cycles (the therapeutic cycle of periodontitis is 7 days, 12.9 is about 2/7 of 45.2) and achieve long-term and stable treatment effectiveness. CA, MCZ, and 5-FU also show the same results, the medicines were released rapidly from SBA-15 and RESIN, and most of the medicines could be trapped in the resin through some strong interactions, resulting in the release being stopped. Further, medicines released from NMCRs experienced two steps. One is the fast-releasing step, resulting in a high concentration of medicine, which could effectively kill bacteria. Then, followed a slow and long-term releasing process with a low medicine concentration, which could effectively inhibit the growth of bacteria.

3.3. In Vitro Studies on Antibacterial Activity and Cell Proliferation. Two birds with one stone were achieved. MINO, CA, and MCZ have biological anti-inflammatory and antibacterial activities, which can effectively inhibit the reproduction of Gram-positive bacteria. 5-FU is an anti-metabolic medicine that is often used to defend cancer. Here, the effects of NMCR@MINO, NMCR@CA, and NMCR@MCZ on defensing common pathogenic bacteria (*Viscous actinomycetes*, *S. mutans*, and *C. albicans*) and the effect of NMCR@5-FU on inhibiting KB cells were investigated. As comparison, the inhibition zones of antibacterial (IZAB) were measured and recorded at 1st, 4th, and 7th days.

Figure 4A displays the antibacterial effects of NMCR@MINO on defending *Viscous actinomycetes*. The diameter of the IZAB is about 18 mm at the 1st day, 16 mm at the 4th day, and 14 mm at the 7th day. Although the length of its diameter was reduced slightly, NMCR@MINO maintained good antibacterial activity still and kept on going. Similarly, Figure 4B,C displays the antibacterial effects of NMCR@CA and NMCR@MCZ on defending *S. mutans* and *C. albicans*. The diameter of the IZAB of NMCR@CA kept about 52 mm and that of NMCR@MCZ kept about 21 mm at the 7th day. All the results confirmed the sustained release of the medicines and showed good antibacterial properties.

https://doi.org/10.1021/acsomega.3c02428
ACS Omega 2023, 8, 23936−23944

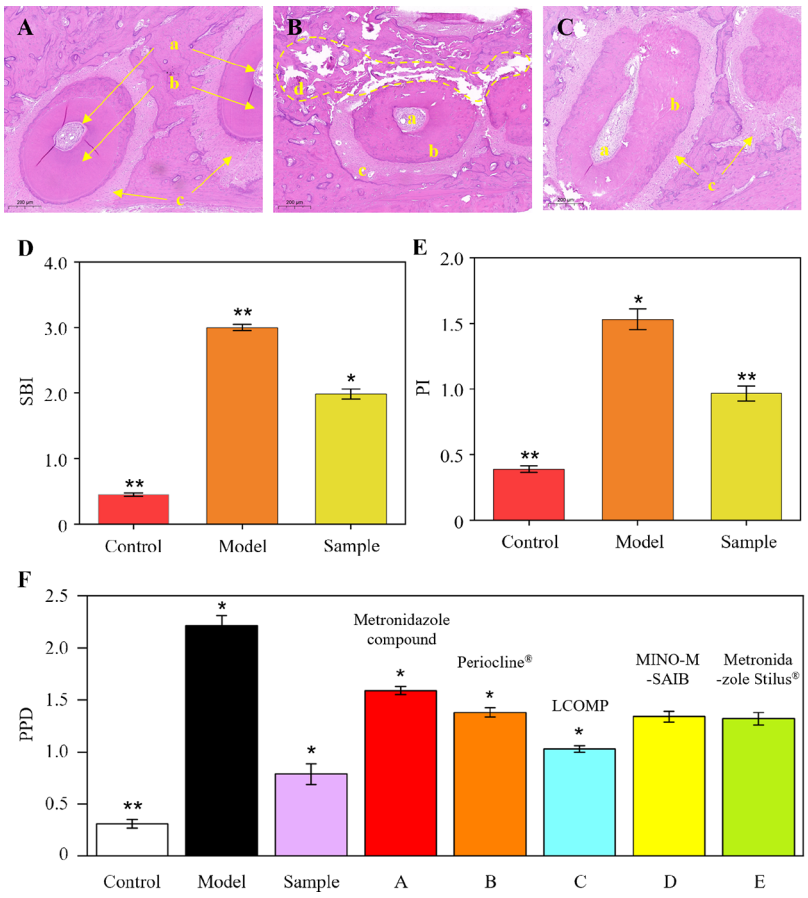

Figure 5. Photograph of dissected molars of rats at the (A) control group, (B) model group, and (C) sample group (labels a, b, c, and d indicate the endodontium, dentin, dental enamels, and periodontal parts, respectively). (D) SBI and (E) PI plots of control, model, and sample groups. (F) Compared PPD plots of control, model, sample groups' and references' results.

Figure 4D compares the percentage of cell growth in the control group (G1 column) and model and sample groups intervened by 5-FU (G2 column) and by NMCR@5-FU (G3 column) at 6, 12, 24, and 48 h. G1 was always 100%, representing the free growth of KB cells without any restrictions. G2 was 53, 86, 96, and 94% to G1 corresponding to the observation at 6, 12, 24, and 48 h. It can be seen that at early time (before 6 h), the 5-FU could limit effectively the growth of KB cells. But with time passing at 12−48 h, 5-FU in the solution had not prevented KB cells from proliferating. That represents 5-FU being rapidly exhausted. The results (G3) of NMCR@5-FU compared with the control group (G1) indicate relative reductions of 92, 83, 68, and 16%. That represents a continuous release of medicine with an appropriate amount and the achievement of long-term and stable restriction on the KB cell growth.

3.4. In Vivo Evaluation of Periodontitis. In vivo therapeutic research against periodontitis was carried on SD rats. Figure S5 shows the procedure of applying NMCR@MINO onto one molar surface of an SD rat. For evaluating the degree of recovery from periodontitis, the comparison of hematoxylin−eosin (HE) staining on the sections along the mesiodistal plane of molars, at a half treatment period of 21 days, was recorded. Figure 5A shows the top observation of dissected molars with healthy endodontium, dentin, and continuous dental enamels of a control rat. All parts could be observed clearly. On the contrary, cementum and tissues infected by periodontitis presented discontinuous dental enamels and broken dentine with a large number of inflammatory and infiltrated cells, wherein the coronal plane of the teeth could easily be found (shown in Figure 5B). Figure 5C displays the observation of the therapeutic result at the half treatment period. With the therapy of NMCR@MINO, although there still were little infected parts, the infiltration of inflammatory cells in dentin was much reduced and the dental enamels returned to be continuous. The periodontal cementum and tissues recovered and new ones grew up. The indicators of the sulcus bleeding index (SBI) and plaque index (PI) on control, sample, and model groups were then checked to verify the status of recovery. As shown in Figure 5D, the SBI value of the control group is 0.47, where the other two values of model and sample groups are 3.00 and 1.90. The PI values are shown in Figure 5E. For the normal rats, the periodontal condition was good, only a small amount of the dental plaque appeared, and the PI value was 0.41. In the rats with chronic periodontitis, a large amount of the thick dental plaque was found at the gingival margin, and the PI value was 1.65. After NMCR@MINO treatment, the number of dental plaques was significantly reduced and the periodontal condition was gradually restored, and the PI value decreased to 0.89. It showed that, with the continuous treatment by MINO released from NMCR, the SBI value reached an average reduction of 36.71% and the PI reached 46.07%. Both the results reflect that the treatment of periodontitis is highly efficient.

Thereafter, the most general indicator of probing pocket depth (PPD) was tested and compared with those from refs 43

https://doi.org/10.1021/acsomega.3c02428
ACS Omega 2023, 8, 23936−23944

and 44 (Figure 5F). The PPD values of control, model, and sample groups were 0.31, 2.23, and 0.69, respectively, which reached a significant average reduction of 69.06%. Compared with some references and two commercial therapeutic varieties, Metronidazole compound, Periocline, LCOMP, MINO-M-SAIB, and Metronidazole Stilus (PPD values about 1.59, 1.38, 1.03, 1.34, and 1.32), the NMCR@MINO appeared to be almost twice as effective as current treatments.

4. CONCLUSIONS

In conclusion, we reported a very simple method of preparing some NMCRs by combining dental resin and MMSs as an in situ spontaneous medicine delivery system. This system allowed a gentle release of medicine molecules from the dual-channel structure that consisted of straight channels of mesoporous SBA-15 and cross-linking networks of composite resin. The developed NMCRs loaded with MINO, CA, MCZ, or 5-FU had excellent antibacterial and anti-inflammatory properties. Taking the in vivo therapy of periodontitis on SD rats as an example, the system (using MINO as the loaded medicine) was proved to greatly improve the speed of healing. We are looking forward to expanding it into an adjunctive promoting strategy of healing other oral diseases, such as dental caries, oral ulcer, buccal mucosa cancer, lip cancers, etc., with in situ, accurate, spontaneous, long-term, stable, and convenient medicine delivery merits.

■ ASSOCIATED CONTENT

Supporting Information

The Supporting Information is available free of charge at https://pubs.acs.org/doi/10.1021/acsomega.3c02428.

SEM images of SBA-15 before and after loading medicines, resin, and NMCR, respectively, SEM-EDS elemental mappings of NMCR, fitting curve of drug release from SBA-15 and resin, and process diagram of using NMCR@MINO on the surface of a molar tooth in an SD rat (PDF)

■ AUTHOR INFORMATION

Corresponding Authors

Jiaping Lu − *Dental Clinic of Xuhui District, Shanghai 200031, People's Republic of China*; Email: natalieljp@126.com

Ka Li − *Institute of Clinical Science, Zhongshan Hospital, Fudan University, Shanghai 200032, People's Republic of China*; Email: karllee75@hotmail.com

Kangjian Tang − *Innovation Center for Chemical Sciences, College of Chemistry, Chemical Engineering and Materials Science and Jiangsu Key Laboratory of Advanced Negative Carbon Technologies, Soochow University, Suzhou 215123, People's Republic of China*; orcid.org/0009-0003-2800-8346; Phone: (+86) 512-6588-0269; Email: kjtang@suda.edu.cn

Authors

Xuan Heng − *Innovation Center for Chemical Sciences, College of Chemistry, Chemical Engineering and Materials Science, Soochow University, Suzhou 215123, People's Republic of China*

Yuhao Pan − *Innovation Center for Chemical Sciences, College of Chemistry, Chemical Engineering and Materials Science, Soochow University, Suzhou 215123, People's Republic of China*

Xinghui Chen − *Innovation Center for Chemical Sciences, College of Chemistry, Chemical Engineering and Materials Science, Soochow University, Suzhou 215123, People's Republic of China*

Liuyi Pu − *Innovation Center for Chemical Sciences, College of Chemistry, Chemical Engineering and Materials Science, Soochow University, Suzhou 215123, People's Republic of China*

Complete contact information is available at: https://pubs.acs.org/10.1021/acsomega.3c02428

Notes

The authors declare no competing financial interest.

■ ACKNOWLEDGMENTS

This work was supported by the National Key Research and Development Program of China (grant no. 2022YFA1503601) and the Jiangsu Shuangchuang Doctor Program (JSSCBS20210676). The authors also thank Ms. Shihui Zheng and Ms. Qingxin Niu for their technical support and some helpful bio-tests from SHIYANJIA Lab.

■ ABBREVIATIONS

MMS, mesoporous molecular sieve; NMCR, nanoporous medical composite resin; COD, chronic oral diseases; MMR, methyl methacrylate resin; MINO, minocycline hydrochloride; CA, clindamycin hydrochloride; MCZ, miconazole nitrate; 5-FU, 5-fluorouracil; TMB, 1,3,5-trimethylbenzene; SD rats, Sprague−Dawley rats; HE, hematoxylin−eosin

■ REFERENCES

(1) Smith, S. L.; Gorantla, R. Analysing the global health agenda: A comparison of priority for diabetes and oral diseases. *Glob. Public Health* **2021**, *16*, 517−531.

(2) Petersen, P. E. Global policy for improvement of oral health in the 21st century - implications to oral health research of World Health Assembly 2007, World Health Organization. *Community Dent. Oral Epidemiol.* **2009**, *37*, 1−8.

(3) Righolt, A. J.; Jevdjevic, M.; Marcenes, W.; Listl, S. Global-, Regional-, and Country-Level Economic Impacts of Dental Diseases in 2015. *J. Dent. Res.* **2018**, *97*, 501−507.

(4) Chen, M. X.; Zhong, Y. J.; Dong, Q. Q.; Wong, H. M.; Wen, Y. F. Global, regional, and national burden of severe periodontitis, 1990-2019: An analysis of the Global Burden of Disease Study 2019. *J. Clin. Periodontol.* **2021**, *48*, 1165−1188.

(5) Dye, B. A. The Global Burden of Oral Disease: Research and Public Health Significance. *J. Dent. Res.* **2017**, *96*, 361−363.

(6) Listl, S.; Galloway, J.; Mossey, P. A.; Marcenes, W. Global Economic Impact of Dental Diseases. *J. Dent. Res.* **2015**, *94*, 1355−1361.

(7) Rajeshwari, H. R.; Dhamecha, D.; Jagwani, S.; Rao, M.; Jadhav, K.; Shaikh, S.; Puzhankara, L.; Jalalpure, S. Local drug delivery systems in the management of periodontitis: A scientific review. *J. Controlled Release* **2019**, *307*, 393−409.

(8) Ding, Q. F.; Cui, J. J.; Shen, H. Q.; He, C. L.; Wang, X. D.; Shen, S. G. F.; Lin, K. L. Advances of nanomaterial applications in oral and maxillofacial tissue regeneration and disease treatment. *Wiley Interdiscip. Rev. Nanomed. Nanobiotechnol.* **2021**, *13*, e1669.

(9) Keller, L. A.; Merkel, O.; Popp, A. Intranasal drug delivery: opportunities and toxicologic challenges during drug development. *Drug Deliv. Transl. Res.* **2022**, *12*, 735−757.

(10) Field, L. D.; Nag, O. K.; Sangtani, A.; Burns, K. E.; Delehanty, J. B. The role of nanoparticles in the improvement of systemic anticancer drug delivery. *Ther. Deliv.* **2018**, *9*, 527−545.
(11) Liu, X. M.; Reinhardt, R. A.; Wang, D. Drug delivery strategies for common orofacial diseases. *J. Drug Targeting* **2006**, *14*, 583−597.
(12) Pihlstrom, B. L.; Michalowicz, B. S.; Johnson, N. W. Periodontal diseases. *Lancet* **2005**, *366*, 1809−1820.
(13) Wang, X.; Ma, J.; Zhu, X.; Wang, F.; Zhou, L. Minocycline-loaded In situ Hydrogel for Periodontitis Treatment. *Curr. Drug Delivery* **2018**, *15*, 664−671.
(14) Garrido-Mesa, N.; Zarzuelo, A.; Galvez, J. Minocycline: far beyond an antibiotic. *Br. J. Pharmacol.* **2013**, *169*, 337−352.
(15) Liang, Y.; Zhao, X.; Hu, T.; Chen, B.; Yin, Z.; Ma, P.; Guo, B. L. Adhesive Hemostatic Conducting Injectable Composite Hydrogels with Sustained Drug Release and Photothermal Antibacterial Activity to Promote Full-Thickness Skin Regeneration During Wound Healing. *Small* **2019**, *15*, 17.
(16) Wang, H.; Chang, X. W.; Ma, Q.; Sun, B. Y.; Li, H.; Zhou, J. M.; Hu, Y. Y.; Yang, X. Y.; Li, J.; Chen, X.; Song, J. L. Bioinspired drug-delivery system emulating the natural bone healing cascade for diabetic periodontal bone regeneration. *Bioact. Mater.* **2023**, *21*, 324−339.
(17) Xue, L.; Deng, T.; Guo, R.; Peng, L.; Guo, J.; Tang, F.; Lin, J.; Jiang, S.; Lu, H.; Liu, X.; Deng, L. A Composite Hydrogel Containing Mesoporous Silica Nanoparticles Loaded With Artemisia argyi Extract for Improving Chronic Wound Healing. *Front. Bioeng. Biotechnol.* **2022**, *10*, 17.
(18) Yin, W. Y.; Yan, L.; Yu, J.; Tian, G.; Zhou, L. J.; Zheng, X. P.; Zhang, X.; Yong, Y.; Li, J.; Gu, Z. J.; Zhao, Y. L. High-Throughput Synthesis of Single-Layer MoS2 Nanosheets as a Near-Infrared Photothermal-Triggered Drug Delivery for Effective Cancer Therapy. *ACS Nano* **2014**, *8*, 6922−6933.
(19) Hasani-Sadrabadi, M. M.; Taranejoo, S.; Dashtimoghadam, E.; Bahlakeh, G.; Majedi, F. S.; VanDersarl, J. J.; Janmaleki, M.; Sharifi, F.; Bertsch, A.; Hourigan, K.; Tayebi, L.; Renaud, P.; Jacob, K. I. Microfluidic Manipulation of Core/Shell Nanoparticles for Oral Delivery of Chemotherapeutics: A New Treatment Approach for Colorectal Cancer. *Adv. Mater.* **2016**, *28*, 4134−4141.
(20) Hua, S. Y.; He, J.; Zhang, F. P.; Yu, J. H.; Zhang, W. X.; Gao, L. Y.; Li, Y. Y.; Zhou, M. Multistage-responsive clustered nanosystem to improve tumor accumulation and penetration for photothermal/enhanced radiation synergistic therapy. *Biomaterials* **2021**, *268*, 19.
(21) Shi, J. J.; Yu, X. Y.; Wang, L.; Liu, Y.; Gao, J.; Zhang, J.; Ma, R.; Liu, R. Y.; Zhang, Z. Z. PEGylated fullerene/iron oxide nanocomposites for photodynamic therapy, targeted drug delivery and MR imaging. *Biomaterials* **2013**, *34*, 9666−9677.
(22) Chen, Z. L.; Huang, M.; Wang, X. R.; Fu, J.; Han, M.; Shen, Y. Q.; Xia, Z.; Gao, J. Q. Transferrin-modified liposome promotes alpha-mangostin to penetrate the blood-brain barrier. *Nanomed.-Nanotechnol. Biol. Med.* **2016**, *12*, 421−430.
(23) Lee, H.; Song, C.; Hong, Y. S.; Kim, M. S.; Cho, H. R.; Kang, T.; Shin, K.; Choi, S. H.; Hyeon, T.; Kim, D. H. Wearable/disposable sweat-based glucose monitoring device with multistage transdermal drug delivery module. *Sci. Adv.* **2017**, *3*, 8.
(24) Nie, D.; Dai, Z.; Li, J.; Yang, Y.; Xi, Z.; Wang, J.; Zhang, W.; Qian, K.; Guo, S.; Zhu, C.; Wang, R.; Li, Y.; Yu, M.; Zhang, X.; Shi, X.; Gan, Y. Cancer-Cell-Membrane-Coated Nanoparticles with a Yolk-Shell Structure Augment Cancer Chemotherapy. *Nano Lett.* **2020**, *20*, 936−946.
(25) Zhou, P.; Xia, Y.; Cheng, X.; Wang, P. F.; Xie, Y.; Xu, S. Enhanced bone tissue regeneration by antibacterial and osteoinductive silica-HACC-zein composite scaffolds loaded with rhBMP-2. *Biomaterials* **2014**, *35*, 10033−10045.
(26) Heikkila, T.; Salonen, J.; Tuura, J.; Kumar, N.; Salmi, T.; Murzin, D. Y.; Hamdy, M. S.; Mul, G.; Laitinen, L.; Kaukonen, A. M.; Hirvonen, J.; Lehto, V. P. Evaluation of mesoporous TCPSi, MCM-41, SBA-15, and TUD-1 materials as API carriers for oral drug delivery. *Drug Delivery* **2007**, *14*, 337−347.
(27) Doadrio, A. L.; Sousa, E. M. B.; Doadrio, J. C.; Pariente, J. P.; Izquierdo-Barba, I.; Vallet-Regi, M. Mesoporous SBA-15 HPLC evaluation for controlled gentamicin drug delivery. *J. Controlled Release* **2004**, *97*, 125−132.
(28) Tang, F. Q.; Li, L. L.; Chen, D. Mesoporous Silica Nanoparticles: Synthesis, Biocompatibility and Drug Delivery. *Adv. Mater.* **2012**, *24*, 1504−1534.
(29) Kim, T. W.; Slowing, I. I.; Chung, P. W.; Lin, V. S. Y. Ordered Mesoporous Polymer-Silica Hybrid Nanoparticles as Vehicles for the Intracellular Controlled Release of Macromolecules. *ACS Nano* **2011**, *5*, 360−366.
(30) Liu, J. J.; Liang, H.; Li, M.; Luo; Zhang, J.; Guo, X.; Cai, K. Tumor acidity activating multifunctional nanoplatform for NIR-mediated multiple enhanced photodynamic and photothermal tumor therapy. *Biomaterials* **2018**, *157*, 107−124.
(31) Zhang, J. F.; Wu, R.; Fan, Y.; Liao, S.; Wang, Y.; Wen, Z. T.; Xu, X. Antibacterial Dental Composites with Chlorhexidine and Mesoporous Silica. *J. Dent. Res.* **2014**, *93*, 1283−1289.
(32) Priyadarsini, S.; Mukherjee, S.; Mishra, M. Nanoparticles used in dentistry: A review. *J. Oral Biol. Craniofac. Res.* **2018**, *8*, 58−67.
(33) Pratap, B.; Gupta, R. K.; Bhardwaj, B.; Nag, M. Resin based restorative dental materials: characteristics and future perspectives. *Jpn. Dent. Sci. Rev.* **2019**, *55*, 126−138.
(34) Pietrella, D.; Marmottini, F.; Padeletti, G.; Montesperelli, G.; Kaciulis, S.; Vici, E.; Cerri, L.; Arnbrogi, V. Resin-Based Materials with Chlorhexidine-Loaded MCM-41: Surface Characteristics, Drug Release, and Antibiofilm Activity. *ACS Biomater. Sci. Eng.* **2018**, *4*, 4144.
(35) Zhao, D.; Feng, J.; Huo, Q.; Melosh, N.; Fredrickson, G.; Chmelka, B.; Stucky, G. D. Triblock copolymer syntheses of mesoporous silica with periodic 50 to 300 angstrom pores. *Science* **1998**, *279*, 548−552.
(36) He, Q.; Zhang, J.; Chen, F.; Guo, L.; Zhu, Z.; Shi, J. An anti-ROS/hepatic fibrosis drug delivery system based on salvianolic acid B loaded mesoporous silica nanoparticles. *Biomaterials* **2010**, *31*, 7785−7796.
(37) Bing, J.; Hu, C.; Nie, Y.; Yang, M.; Qu, J. Mechanism of Catalytic Ozonation in Fe_2O_3/Al_2O_3@SBA-15 Aqueous Suspension for Destruction of Ibuprofen. *Environ. Sci. Technol.* **2015**, *49*, 1690−1697.
(38) Trendafilova, I.; Szegedi, A.; Mihaly, J.; Momekov, G.; Lihareva, N.; Popova, M. Preparation of efficient quercetin delivery system on Zn-modified mesoporous SBA-15 silica carrier. *Mater. Sci. Eng. C-Mater. Biol. Appl.* **2017**, *73*, 285−292.
(39) Rauta, P. R.; Das, N. M.; Nayak, D.; Ashe, S.; Nayak, B. Enhanced efficacy of clindamycin hydrochloride encapsulated in PLA/PLGA based nanoparticle system for oral delivery. *IET Nanobiotechnol.* **2016**, *10*, 254−261.
(40) Kazmi, S. A. R.; Qureshi, M. Z.; Sadia; Alhewairini, S. S.; Ali, S.; Khurshid, S.; Saeed, M.; Mumtaz, S.; Mughal, T. A. Minocycline-Derived Silver Nanoparticles for Assessment of Their Antidiabetic Potential against Alloxan-Induced Diabetic Mice. *Pharmaceutics* **2021**, *13*, 19.
(41) Hsin, Y. K.; Thangarajoo, T.; Choudhury, H.; Pandey, M.; Meng, L. W.; Gorain, B. Stimuli-Responsive in situ Spray Gel of Miconazole Nitrate for Vaginal Candidiasis. *J. Pharm. Sci.* **2023**, *112*, 562−572.
(42) He, J.; Luo, Y.; Liu, F.; Jia, D. Synthesis, Characterization and Photopolymerization of a New Dimethacrylate Monomer Based on (alpha-Methyl-benzylidene)bisphenol Used as Root Canal Sealer. *J. Biomater. Sci.-Polym. Ed.* **2010**, *21*, 1191−1205.
(43) Liu, R.; Li, N.; Liu, N.; Zhou, X.; Dong, Z. M.; Wen, X. J.; Liu, L. C. Effects of systemic ornidazole, systemic and local compound ornidazole and pefloxacin mesylate on experimental periodontitis in rats. *Med. Sci. Monit.* **2012**, *18*, BR95−BR102.
(44) Zhang, T.; Qiu, Y.; Song, J.; Zhou, P.; Liao, H.; Cheng, Y.; Wu, X. Electrosprayed minocycline hydrochloride-loaded microsphere/SAIB hybrid depot for periodontitis treatment. *Drug Delivery* **2021**, *28*, 620−633.

https://doi.org/10.1021/acsomega.3c02428
ACS Omega 2023, 8, 23936−23944